actuators

MDPI

Article

Minitype Arrays of Acoustically Actuated Magnetoelectric Antennas for Magnetic Induction Communication

Shiyu Wang [1], Gaoqi Dou [1,*] and Guangming Song [2]

[1] College of Electronic Engineering, Naval University of Engineering, Wuhan 430033, China; wangshiyuestc@163.com
[2] School of Aerospace Engineering, Tsinghua University, Beijing 100084, China; sgm21@mails.tsinghua.edu.cn
* Correspondence: hjgcqq@163.com

Abstract: The magnetoelectric (ME) antennas rely on the mechanical movement of magnetic dipoles, making it possible to break the constraints on physical dimensions decided by the wavelength of the electromagnetic wavelength. The ME antennas achieve super-low frequency (SLF) communications with a smaller size to provide a novel solution for long-range, underwater, and underground communications; navigation over the horizon; and geological exploring. As a result, further theoretical research and optimization of ME antennas have been an open challenge for decades. Here, we report on minitype arrays of acoustically actuated ME antenna and their more rigorous equivalent circuits. These arrays of ME antenna adjust amplitude-frequency response through the mechanical regulation method. The mechanical parameters of ME antennas in the arrays result in regulating amplitude-frequency response, such as working frequency, fractional bandwidth, and intensity of magnetic induction. Our work provides a more accurate theoretical model and diverse array form over state-of-the-art ME antenna arrays. The frequency, fractional bandwidth, and magnetic induction strength of the ME antenna arrays were achieved to be adjustable in the ranges of 84 to 181 Hz, 3.9% to 8.3%, and two to four times, respectively. In addition, we have calculated the attenuation characteristics of ME antennas and their minitype arrays in seawater. The results show that the ME antenna array described in this manuscript is able to enhance the radiation intensity and information-loading capability, which has a positive potential for application in SLF communication systems.

Keywords: minitype arrays; magnetoelectric antenna; equivalent circuit; mechanical regulation

check for updates

Citation: Wang, S.; Dou, G.; Song, G. Minitype Arrays of Acoustically Actuated Magnetoelectric Antennas for Magnetic Induction Communication. *Actuators* **2024**, *13*, 276. https://doi.org/10.3390/act13080276

Academic Editors: Biao Xiang, Cong Peng and Haitao Li

Received: 21 June 2024
Revised: 18 July 2024
Accepted: 22 July 2024
Published: 23 July 2024

Copyright: © 2024 by the authors. Licensee MDPI, Basel, Switzerland. This article is an open access article distributed under the terms and conditions of the Creative Commons Attribution (CC BY) license (https://creativecommons.org/licenses/by/4.0/).

1. Introduction

Super-low frequency (SLF, 30–300 Hz) electromagnetic (EM) waves have the advantages of strong stability, long propagation distance, and low attenuation in the conductive medium [1,2]. They have been widely used in geological surveys, seismic research, navigation, underground communication, and submarine communication. Especially in the field of submarine communication, SLF electromagnetic waves can solve the problem of long-distance and large-depth communication between land-based stations and underwater vehicles [3].

Compact antennas rely on an EM wave resonance and typically have a size of more than $\lambda_0/10$, which is one-tenth of the EM wavelength λ_0. The limitation on antenna size miniaturization has made it very challenging to achieve compact antennas and antenna arrays, particularly at low frequency (LF, below 300 kHz) with large λ_0, thus severely limiting wireless communication systems on underwater vehicles and land-based stations [4]. The acoustically actuated magnetoelectric (ME) antennas have a new receiving and transmitting mechanism for EM waves to break the dimensions limit [5–12]. Compared with the existing low-frequency transmitting antennas, the size of ME antennas has been significantly reduced. Figure 1 shows the size comparison of existing low-frequency antennas and ME antennas. Compared with other types of mechanical antennas, ME antennas have the advantages of high flexibility and easy regulation [6].

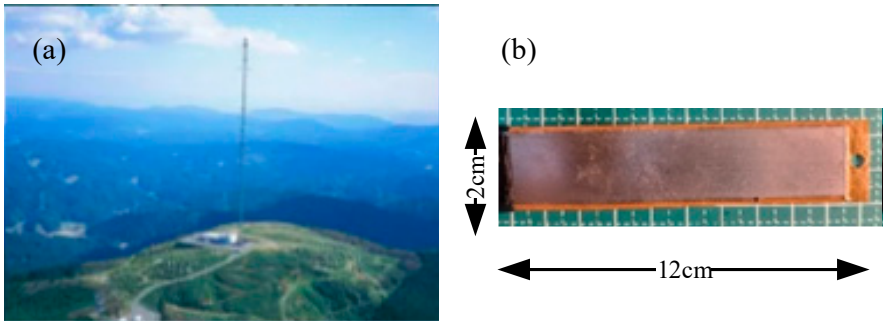

Figure 1. The size comparison of existing low-frequency antennas and ME antennas: (**a**) The existing low-frequency antennas. (**b**) The ME antennas.

Current research on ME antennas' transmission distance mainly focuses on the following aspects: enhancing the radiation capability of one ME antenna [13–21] and combining the ME antennas into an array [22–24]. However, the radiation ability of one ME antenna is limited, and the goal of long-distance transmission cannot be achieved.

Many researchers currently choose to form an array of mechanical antennas to obtain greater radiation capacity, but there is no accurate theoretical support [22–26]. Here, one question naturally arises: is it possible to provide theoretical guidance for the frequency response radiation and efficiency calculation of the arrayed ME antenna? Based on our results in this work, we can answer this question affirmatively.

ME antenna, as a new type of antenna based on multi-physical field coupling such as electric-mechanical-magnetic, solves the problem of miniaturization of low-frequency antennas and at the same time brings some difficulties to the traditional antenna field, such as frequency reconfiguration, bandwidth reconfiguration, grouping arrays, and so on. The traditional research method of the electric antenna is no longer suitable for solving the multi-physics field problems, so it is a shortcut to seek a solution to the difficult problems of the ME antenna in the non-electromagnetic domains such as the mechanical domain and other physical fields. The methodology diagram of this paper is shown in Figure 2.

As early as 2005, some researchers proposed a simple equivalent circuit model of ME antenna for qualitative analysis of series structure and parallel structure [22]. Some researchers have been able to adjust the frequency response of ME antennas by means of parallel arrays, but no theoretical guidance similar to the equivalent circuit model has been proposed [23]. In 2022, some researchers established series and parallel arrays of ME antennas and their equivalent circuit models, which provided accurate theoretical guidance for adjusting the frequency response but did not carry out the derivation of the correspondence between the circuit and the mechanical domain [24].

Compared with the research performed by other researchers in the ME antenna array, the ME antenna array and its equivalent circuit described in our work have many improvements, as shown in Table 1.

Our work provides a detailed derivation of the correspondence between the various parameters of the mechanical domain and the parameters in the equivalent circuit. The corresponding series–parallel relationships in the mechanical domain and circuits are also well proven. Note that our work also uses the relationship between the work conducted by different forces in simple harmonic vibration to establish an equivalent model and formula for calculating the mechanical vibration (EMV). Based on the series and parallel ME antennas established by predecessors, we combine the advantages of series and parallel arrays and innovatively design a quaternary series–parallel stacked antenna array.

Here, we demonstrate the small arrays operating at SLF and ULF frequencies based on the multi-physics coupling of electric, mechanical, and magnetic fields, including binary series arrays, binary parallel arrays, and quaternary series–parallel stacked arrays of ME antennas. The frequency responses of these arrays can be accurately calculated by equivalent circuit models. During the transmitting process, the ME antennas produce an oscillating me-

chanical strain under an alternating voltage input, which mechanically excites the magnetic layer and induces a magnetization oscillation that radiates EM waves [5–24]. Therefore, these ME antennas operate at their acoustic resonance instead of EM resonance. Since the vibration of the ME antenna is affected by mechanical parameters such as damping, mechanical load, and elastic coefficient, its frequency response can be accurately expressed by these parameters. Then, the equivalent circuit of the ME antenna can be expressed by parameters such as resistance, inductance, and capacitance in the resonant circuit. We can accurately calculate the frequency response of the ME antenna array based on the equivalent circuit. These minitype arrays are expected to have sizes comparable to the single ME antennas, thus leading to the large-scale array consisting of minitype arrays with greater radiation capability, compared to state-of-the-art ME antenna arrays.

The contents of this paper are organized as follows. In Section 2, based on the vibration theory, mechanics principle, and circuit philosophy, the series–parallel relationship of the ME antenna in the mechanical domain and circuit was qualitatively analyzed. Based on this quantitative relationship, the equivalent circuit model of the ME antenna and its arrases were established. In Section 3, according to the theoretical analysis, the minitype arrays of ME antenna based on the series–parallel relationship were designed. In Section 4, the frequency response and pattern of the arrays were measured, respectively, for validation. The conclusions drawn are outlined in Section 5.

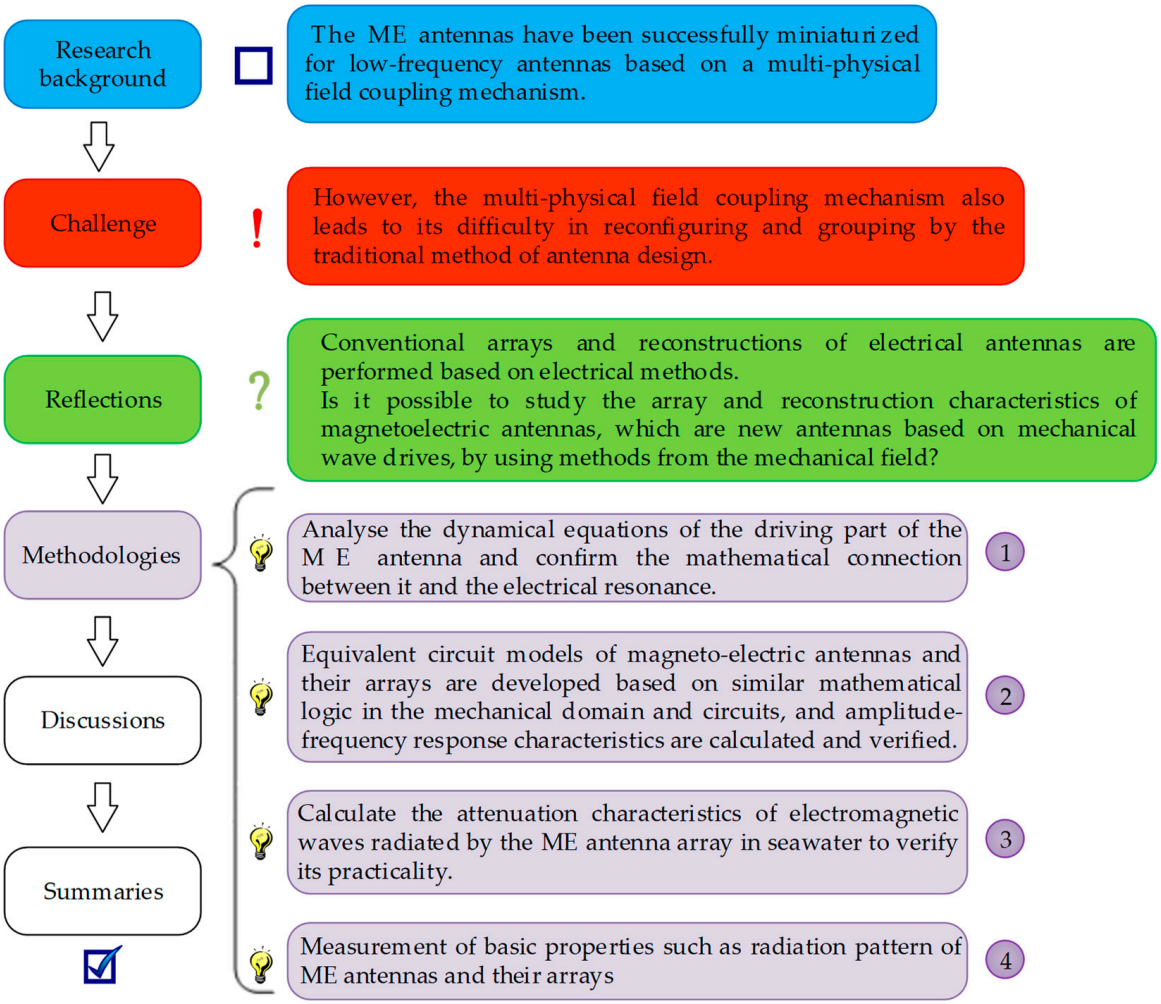

Figure 2. The methodology diagram of this paper.

Table 1. A comparison of state-of-the-art ME antenna arrays.

Reference	Frequency Range	The Form of the Array	Methods	Progress
[22]	40–140 KHz	1. In series 2. In parallel	Simple equivalent circuit	Qualitative analysis of the ME effect
[23]	7.9 KHz	Spaced arrangement in parallel	—	1. Adjustment of the frequency response 2. Doubling the bandwidth
[24]	20–30 KHz	1. In series 2. In parallel	Equivalent circuit	1. Adjustment of the frequency response 2. Doubling the bandwidth
Our work	SLF	1. In series 2. In parallel 3. Series–parallel stack	1. The equivalent circuit used to calculate the frequency response 2. The equivalent circuit used to calculate the EMV	1. Adjustment of the frequency response 2. Calculation of the EMV

2. Mechanical Model and Equivalent Circuit Model of ME Antenna

One typical ME antenna and three types of original minitype arrays were employed for the study, which are shown in Figure 3.

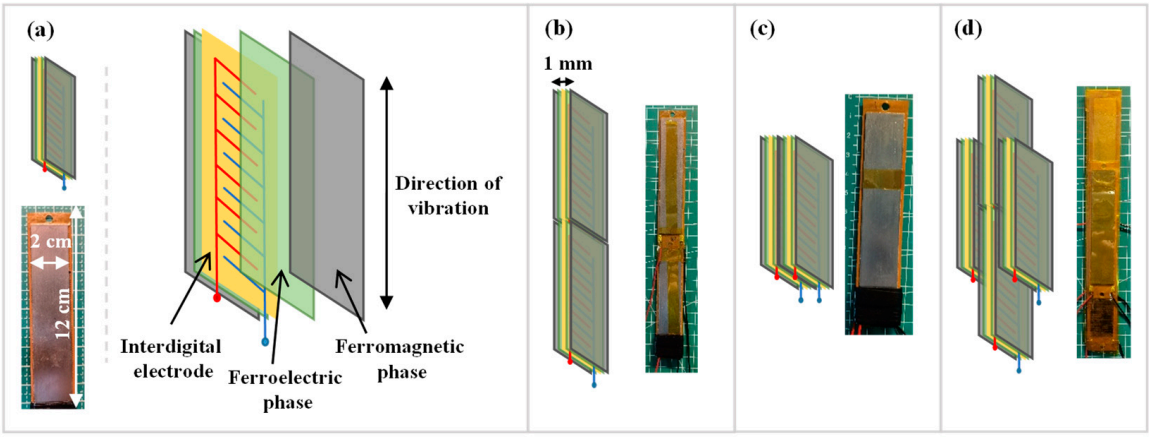

Figure 3. The configuration of the ME antenna and its arrases under study: (**a**) The configuration of the ME antenna. (**b**) The configuration of the binary series array (BSMEA). (**c**) The configuration of the binary parallel array (BPMEA). (**d**) The configuration of the quaternary series–parallel stack array (QSPMEA).

The typical ME antenna includes the ferroelectric phase film, the ferromagnetic phase film, and the embedded driven interdigital electrode film [5–24]. The input electrical signal will be converted into vibration along the length direction by the ME antenna and its array and will finally generate the radiating magnetic field. The above process is a typical multi-physics coupling associated with the electric, mechanical, and magnetic fields. The binary series array of ME antenna (BSMEA) comprises two identical ME antennas along the vibration direction, as shown in Figure 3b. The binary parallel array of ME antenna (BPMEA) comprises two identical ME antennas in the orthogonal direction along the vibration direction, as shown in Figure 3c. The quaternary series–parallel stack array of ME antenna (QSPMEA) is composed of two identical ME antennas in parallel at the interface based on the binary series array of ME antenna, as shown in Figure 3d.

The equivalent models of ME antenna arrays are constructed regarding the following three aspects to understand the key parameters in determining their frequency responses and efficiency of EMV.

2.1. Series–Parallel Relationship of ME Antenna

Combined with the analysis of Newton's second law and Hooke's law on simple harmonic vibration objects [27,28], it can be known that the vibration frequency (f) of the ME antenna is expressed by the load mass (m) and the elastic coefficient (k):

$$f_0 = \frac{1}{2\pi}\sqrt{\frac{k_0}{m_0}} \tag{1}$$

The energy consumption is related to the damping coefficient (r) in the actual vibration process. The quality factor (Q) is derived according to the ratio of total energy and damping energy consumption, which can be simplified as:

$$Q = \frac{k_0}{2\pi r_0 f_0} \tag{2}$$

Then, the bandwidth (B) can be calculated as:

$$B = \frac{f_0}{Q} = \frac{r_0}{2\pi m_0} \tag{3}$$

Although the resonant frequency and bandwidth can be predicted by Equations (1) and (3), the equations only describe the mechanical vibration. As for the antenna, the electromagnetic radiation and its regulation method are directly understood from the mechanical domain illustration. To fill the gap between the mechanical model and the EM radiation, the equivalent circuit model (ECM) is developed. Note that Equation (3) can be rewritten as:

$$f_0 = \frac{1}{2\pi}\sqrt{\frac{1}{m_0 {k_0}^{-1}}} \tag{4}$$

which is similar to the formula for solving the resonant frequency of the LC circuit. The above formula has the same calculation logic as that of the resonant circuit. Therefore, the electromechanical-electromagnetic multi-physical process of the ME antenna can be simplified by the method of equivalent circuits.

First, we assume that in the mechanical domain, the series relationship means that the ME antennas are connected along the vibration direction, as shown in Figure 3b. The parallel relationship means that the ME antennas are connected in the orthogonal direction of the vibration direction, as shown in Figure 3c. Here, one question naturally arises: how do the load mass, elastic coefficient, and damping in the mechanical domain correspond to the parameters in the LC circuit? Based on the mechanical analysis of the ME antenna, we can answer this question affirmatively.

Combined with Hooke's law, in the mechanical domain, when multiple ME antennas are in series, the relationship between the total elastic coefficient and the elastic coefficients of each ME antenna is $k^{-1} = {k_1}^{-1} + {k_2}^{-1} + {k_3}^{-1} + \ldots$. When multiple ME antennas are in parallel, the relationship between the total elastic coefficient and the elastic coefficients of each ME antenna is $k = k_1 + k_2 + k_3 + \ldots$ It has the same form as the equivalent capacitance of multiple capacitors in the LC circuit.

The mass is a scalar without direction. So, no matter how the ME antenna is combined, its load mass is cumulative. As shown in Figure 4, the resistance of the ME antenna in the vibration is the product of velocity and damping.

Combined with Newton's second law, when the vibration direction is constant, the resistance of ME antennas is cumulative regardless of series or parallel. With the same vibration amplitude (x) and velocity (v), the energy (E_r) consumed by damping is the same in series and parallel systems. So, no matter how the ME antenna is combined, its damping is cumulative when the velocity of its vibration is constant. Unlike load mass, damping is the only physical quantity that consumes energy in the vibration system of ME antennas.

In summary, the load mass (m) and damping (r) are equivalent to the inductance (L) and resistance (R) in the LC resonant circuit, respectively. Note that, the load mass and damping are cumulative regardless of whether the ME antennas are connected in series or parallel.

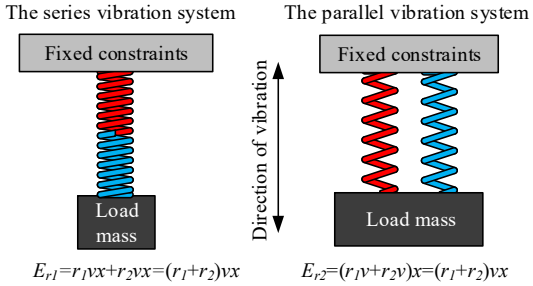

Figure 4. The damping analysis of series and parallel vibration systems.

2.2. Equivalent Circuit Model of ME Antenna Arrays

From the above correspondence, the working frequency and bandwidth can be calculated by:

$$f_0 = \frac{1}{2\pi}\sqrt{\frac{1}{L_0 C_0}} \tag{5}$$

$$B = \frac{R_0}{2\pi L_0} \tag{6}$$

Combined with the derivation process in Table 2, we can see that the series–parallel relationship of the elastic coefficient is opposite to the series–parallel relationship of the equivalent capacitance.

Table 2. The correspondence between elastic coefficient and equivalent capacitance [27,28].

	Derivation Step 1	**Derivation Step 2**	**Derivation Step 3**
Series capacitor	$C_s = \frac{C_1 C_2}{C_1+C_2}$	$C = k^{-1}$	$C_s = (k_1 + k_2)^{-1} = {k_p}^{-1}$
Parallel capacitance	$C_p = C_1 + C_2$		$C_p = (\frac{k_1 k_2}{k_1+k_2})^{-1} = {k_s}^{-1}$
Series elastic coefficient	$k_s = \frac{k_1 k_2}{k_1+k_2}$		$k_s = (C_1 + C_2)^{-1} = {C_p}^{-1}$
Parallel elastic coefficient	$k_p = k_1 + k_2$		$k_p = (\frac{C_1 C_2}{C_1+C_2})^{-1} = {C_s}^{-1}$

From good agreement between the mechanical and the equivalent circuit, it has the same form in depicting the oscillation/resonance. Therefore, the equivalent circuit of ME antenna arrays can use the law in the series–parallel circuits as a reference. The equivalent circuit model of the ME antenna and its arrays are shown in Figure 5.

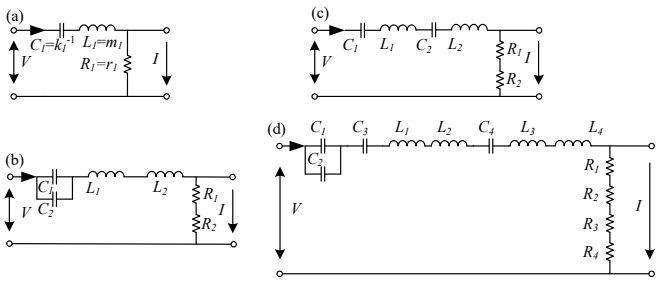

Figure 5. The equivalent circuit model of the ME antenna and its arrays: (**a**) The equivalent circuit of the ME antenna. (**b**) The equivalent circuit of BSMEA. (**c**) The equivalent circuit of BPMEA. (**d**) The equivalent circuit of QSPMEA.

2.3. Equivalent Circuit Model Used to Calculate the Efficiency of Mechanical Vibration

The equivalent circuit used to calculate the frequency response above does not have the concept of radiation resistance. This is because only damping consumes energy in full-cycle simple harmonic vibration, and the energy consumed by damping is not the energy radiated. The EMV of the ME antenna can be obtained by considering the elastic force and damping force to do work. The expressions for the work performed by elastic force (E_k) and the work performed by damping force (E_l) are as follows [29–33]:

$$E_k = kx^2 \tag{7}$$

$$E_l = rvx = rfx^2 \tag{8}$$

In which x represents the vibration amplitude, and v represents the velocity of the vibration. The above two equations are similar to the expression of energy consumed by resistors in a circuit:

$$E = I^2R \tag{9}$$

The equivalent circuit of the ME antenna for calculating the EMV can be obtained by equating the amplitude of the mechanical motion of the ME antenna (x) to the amplitude of the current in the circuit (I), the elastic coefficient (k) to the radiation resistance (R_k), and the product of the damping force and frequency (r_f) to the loss resistance (R_l). The equivalent circuit is shown in Figure 6.

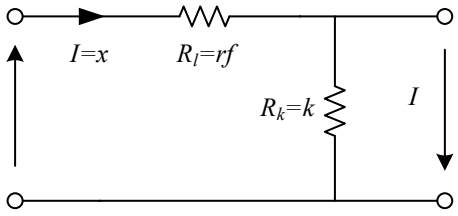

Figure 6. The equivalent circuit is used to calculate the EMV.

In summary, the EMV expression of the ME antenna can be obtained as follows:

$$\eta = \frac{E_k}{E_k + E_l} = \frac{k}{k + rf} \tag{10}$$

Because the ME antennas in the arrays are independently powered, and their mechanical parameters do not affect each other, the EMV of the array is consistent with that of a single array element. Taking the single ME antenna in the resonant state (f = 182 Hz) as an example, its EMV is as follows:

$$\eta = \frac{k}{k + rf} = \frac{9276}{9276 + 0.3 \times 182} \approx 99.4\% \tag{11}$$

3. Theoretical Electromagnetic Field Distribution

Figure 7 illustrates the equivalent magnetic dipole model of the ME antenna and its array.

The ME antennas can generally be equated to a vibrating magnetic dipole, as shown in Figure 6a, during vibration along the magnetization direction. Figure 6b shows the theoretical model of BSMEA. Figure 6c shows the theoretical model of BPMEA. Figure 6d shows the theoretical model of QPSMEA. The *Z*-axis direction in Figure 6 is the magnetization direction and vibration direction of the ME antenna and its array.

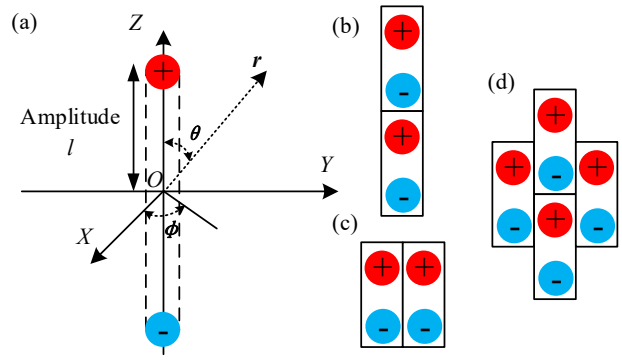

Figure 7. The theoretical model of the ME antenna and its arrays: (**a**) The theoretical model of the ME antenna. (**b**) The theoretical model of BSMEA. (**c**) The theoretical model of BPMEA. (**d**) The theoretical model of QSPMEA.

3.1. The Electromagnetic Field Expression of ME Antenna

For the ME antennas, assuming that their vibration amplitude along the magnetization direction is l, the magnetized equal amount of dissimilar magnetic charge (Q) at both ends and the frequency of vibration is f. The expression for the magnetic dipole moment of the magnetic dipole (m) along the Z-axis in Figure 6a is given by:

$$\mathbf{m} = Ql\cos(2\pi ft)\hat{z} \tag{12}$$

Let $|\mathbf{m}| = \mathrm{m}$, and the following initial variables are set:

$$\begin{cases} B_0 = \mu_0 k^3 m/4\pi \\ E_0 = \eta_0 k^3 m/4\pi \end{cases} \tag{13}$$

where μ_0 is the relative permeability of free space, η_0 is the wave impedance in free space, and k is the wave number. According to the electromagnetic theory, the time-varying magnetic/electric field components generated by the vibrating magnetic dipole can be obtained as follows:

$$\mathbf{B} = B_0 e^{-jkr}\left\{\begin{array}{c} 2\left[\mathrm{j}/(kr)^2 + 1/(kr)^3\right]\cos\theta\mathbf{r} - \\ \left[1/(kr) - \mathrm{j}/(kr)^2 - 1/(kr)^3\right]\sin\theta\boldsymbol{\theta} \end{array}\right\} \tag{14}$$

$$\mathbf{E} = E_0 e^{-jkr}\left[1/(kr) - \mathrm{j}/(kr)^2\right]\sin\theta\boldsymbol{\varphi} \tag{15}$$

From the above equation, it can be seen that there are three attenuation terms in ME antennas. According to the value of kr taken, it can be categorized into near-field, intermediate, and far-field regions.

In the near-field region, since $kr << 1$, e^$(-jkr) \approx 1$, the higher powers of $(1/kr)$ will play a major role. Based on the magnetic dipole model, the near-field magnetic and electric fields of the ME antennas are expressed as:

$$\mathbf{B}_{near} \approx \mu_0 m/(4\pi r^3)\cdot[2\cos\theta\mathbf{r} + \sin\theta\boldsymbol{\theta}] \tag{16}$$

$$\mathbf{E}_{near} \approx -\mathrm{j}\mu_0 mf/(2r^2)\cdot\sin\theta\boldsymbol{\varphi} \tag{17}$$

From the above equation, the magnetic field in the near zone of a vibrating magnetic dipole has both r and θ components, whose amplitude is proportional to m/r^3 and which have a maximum near-zone field at $\theta = 0$ (Z-axis).

In the far-field region, since $kr >> 1$, $(1/kr)$ will play a major role. Let $\omega = 2\pi f$, and then the magnetic and electric fields of the ODMEA can be expressed as:

$$\mathbf{B}_{far} \approx -\mu_0\omega^2 m/(4\pi c^2 r)\cdot e^{-\mathrm{j}kr}\sin\theta\boldsymbol{\theta} \tag{18}$$

$$\mathbf{E}_{far} \approx \eta_0 \omega^2 m/(4\pi c^2 r) \cdot e^{-\mathrm{j}kr} \sin\theta \boldsymbol{\varphi} \tag{19}$$

From the above equation, it can be seen that the far region of the vibrating magnetic dipole has only θ or φ components, and its far-region electric/magnetic fields are spherical waves whose amplitudes decay with $1/r$ and are in-phase, and at this time the energy is completely radiated.

The radiated power (P) of the ME antennas can be expressed by the Poynting vector ($\mathbf{S}$) as follows:

$$P = \oint |\mathbf{S}| r^2 \mathrm{d}\Omega \approx 20\omega^4 m^2/c^4 \tag{20}$$

3.2. Attenuation Characteristics of the ME Antenna and Its Arrays in Seawater

Based on the FEKO 2021.1 electromagnetic simulation software, the attenuation characteristics of the ME antenna and its array in seawater at their respective resonant frequencies can be calculated, as shown in Figure 8.

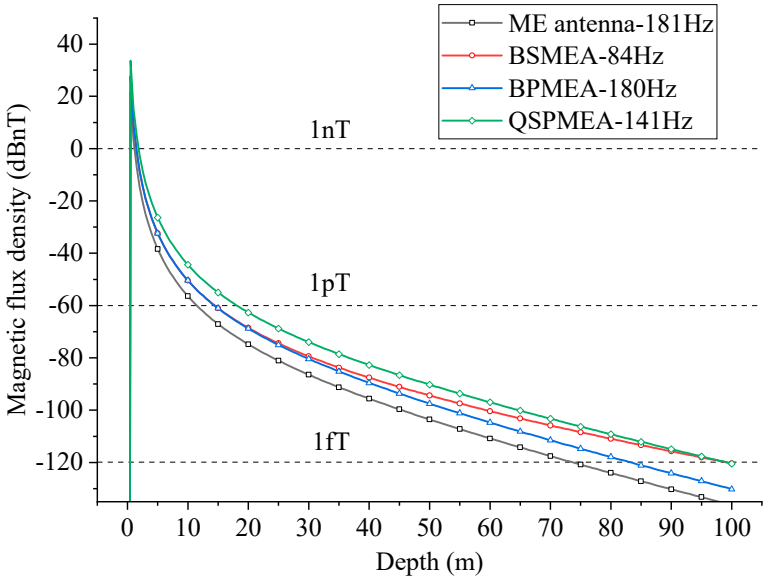

Figure 8. Attenuation characteristics of ME antenna and its arrays in seawater.

The output of the equivalent magnetic dipole in the FEKO is adjusted based on the measured data at the initial point location (0.9 m), and thus the attenuation characteristics of different antenna arrays have been calculated.

The results show that BSMEA and QSPMEA are capable of generating a magnetic induction strength of 1 fT at 100 m underwater. Among them, the BSMEA has a lower resonance frequency and has less attenuation in seawater. The QSPMEA generates a larger magnetic induction strength, leading to a longer transmission distance. With the support of existing sensor technology, it is possible to achieve SLF communication at 100 m underwater.

4. Experimental System and Measurement Results

From the above, the three arrays demonstrate that the resonant frequency and fractional bandwidth can be reconfigured. In this section, we tested the amplitude-frequency response and the radiation pattern of the three arrays, using the experimental platform shown in Figure 9. A schematic diagram of the test equipment is given in Figure 10.

The signals generated by the signal generator are transmitted to the ME antenna through the power amplifier. The ME antenna, under the condition of magnetic bias provided by the Helmholtz coil, converts the electrical field to mechanical waves, and then into the magnetic field. The magnetic field is radiated and is then captured by the

magnetic sensor. Next, the information from the magnetic sensor is sent to the frequency spectrum analyzer. The sensor bracket (shown in Figure 9) can fix the sensor at different positions to measure the radiation pattern of the antenna to be tested in the reference coordinate system.

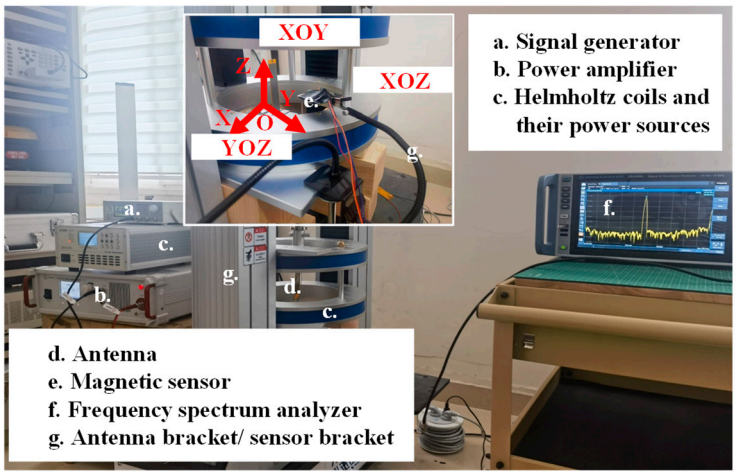

Figure 9. Test equipment for ME antennas.

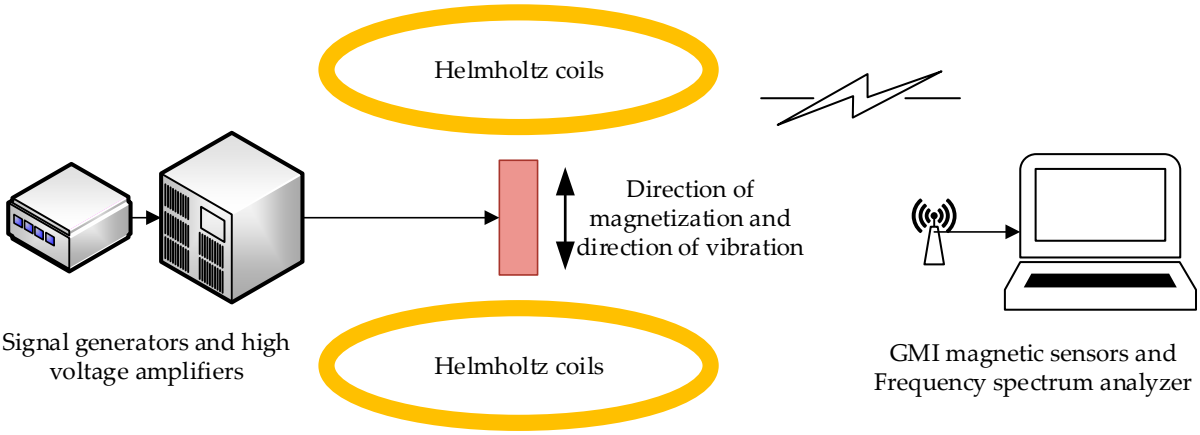

Figure 10. A schematic diagram of the test equipment.

The amplitude-frequency response characteristics can be derived by measuring the magnetic induction strength generated by the ME antenna (0.9 m) under the condition of input signals of different frequencies. The theoretical value of the amplitude-frequency response is derived from the equivalent circuit model. The test results verify the precise tuning of the amplitude-frequency response characteristics of the ME antenna array.

By measuring the magnetic induction strength produced by the antenna at different angles and normalizing it, the radiation pattern of the antenna was obtained. The test results show that the ME antenna and its array have a radiation pattern that approximates that of an equivalent magnetic dipole.

The elements in the three arrays are fed independently. All the data in the three design schemes are the same as those in Table 3.

Table 3. The required physical parameters of the three ME antenna arrays.

	Single ME Antenna	BSMEA	BPMEA	QSPMEA
Elastic coefficient k_s (N/m)	9276	4638	18,551	23,189
Equivalent capacitance C (F)	0.000107	0.000216	0.000054	0.000043
Mechanical load m_s (kg)	0.007	0.014	0.014	0.028
Equivalent inductance L (H)	0.007	0.014	0.014	0.028
Damping r_s (N/(m/s))	0.3	0.6	0.6	1.2
Equivalent resistance R (Ω)	0.3	0.6	0.6	1.2

The results show that the resonant frequency of the QSPMEA is reduced to 141 Hz, the fractional bandwidth is extended to 5.0%, and the magnetic field density is improved by 12 dB compared to the single ME antenna. Moreover, due to the large coupling area of the two ME antennas, the theoretical and test results are in good agreement.

All the test data for ME antennas and three array antennas are shown in Table 4.

Table 4. The test results of the three ME antenna arrays.

	Single ME Antenna	BSMEA	BPMEA	QSPMEA
Resonant frequency (Hz)	181	84	180	141
Bandwidth (Hz)	7	7	7	7
Fractional bandwidth	3.9%	8.3%	3.9%	5.0%
Magnetic induction intensity (dBnT)	10.4	16.4	16.7	22.8

In the ME antenna array, each array element is powered independently, so the EMV of the array is consistent with that of the single ME antenna.

In general, the three ME antenna arrays have different advantages in addition to improving the radiation intensity. The binary series array of the ME antenna can greatly reduce the resonant frequency and increase the fractional bandwidth. The binary parallel array of the ME antenna has low error and good coupling. The quaternary series–parallel stack array of the ME antenna can combine the advantages of the above two arrays, generate four times the radiation intensity, reduce the resonant frequency, increase fractional bandwidth, and have good coupling.

4.1. BSMEA

This section tests the frequency response and radiation pattern of the BSMEA, and the results are shown in Figure 11. The results show that the resonant frequency of the BSMEA is reduced to 84 Hz, the fractional bandwidth is extended to 8.3%, and the magnetic field density is improved by 6 dB compared to the single ME antenna. However, due to the small coupling area of the two ME antennas, there are some errors in the BSMEA's theoretical and measured frequency responses. The theoretical and test results of the radiation pattern are in good agreement.

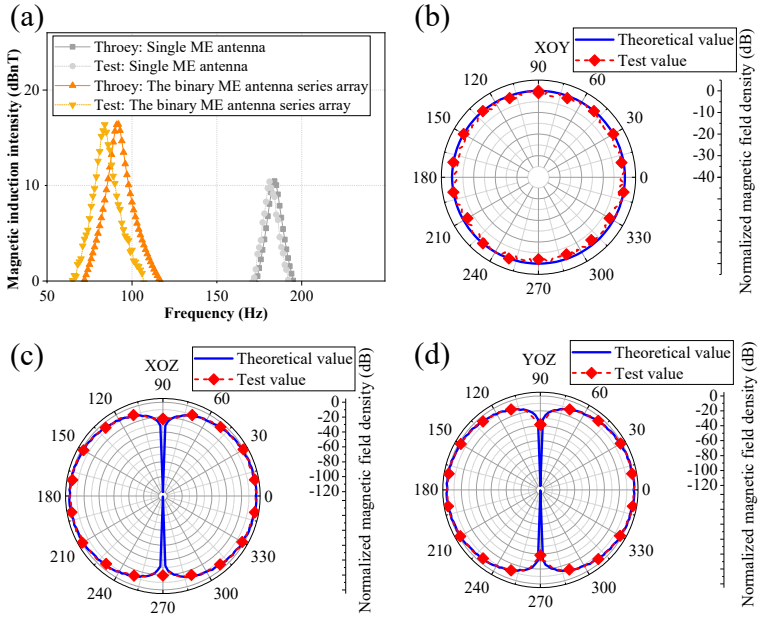

Figure 11. Test results of the binary series array of ME antenna: (**a**) The frequency response of the binary series of ME antenna. (**b**) The radiation pattern of the XOY plane. (**c**) The radiation pattern of the XOZ plane. (**d**) The radiation pattern of the YOZ plane.

4.2. BPMEA

This section tests the frequency response and radiation pattern of the BPMEA, and the results are shown in Figure 12. The results show that the resonant frequency and fractional bandwidth of the BPMEA are unchanged, and the magnetic induction is improved by 6 dB compared to the single ME antenna. Moreover, due to the large coupling area of the two ME antennas, the theoretical and test results are in good agreement.

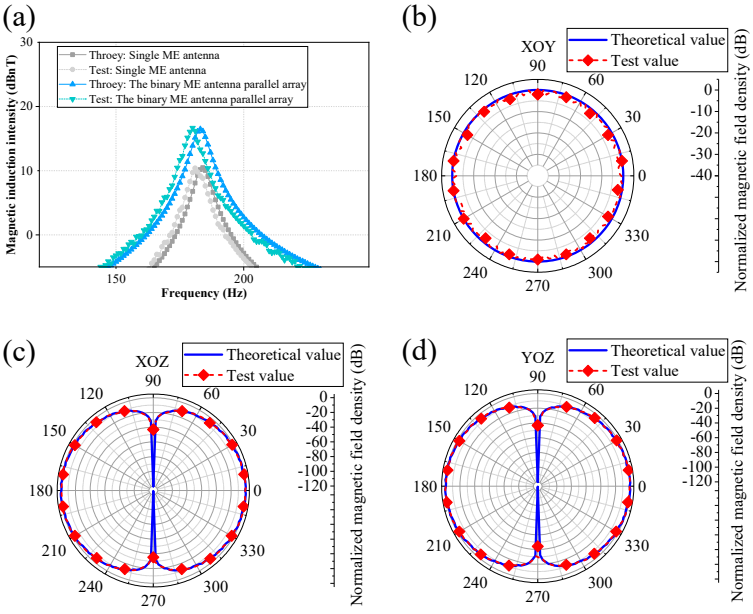

Figure 12. Test results of the binary parallel array of ME antenna: (**a**) The frequency response of the binary parallel of ME antenna. (**b**) The radiation pattern of the XOY plane. (**c**) The radiation pattern of the XOZ plane. (**d**) The radiation pattern of the YOZ plane.

4.3. QSPMEA

This section tests the frequency response and radiation pattern of the QSPMEA, and the results are shown in Figure 13.

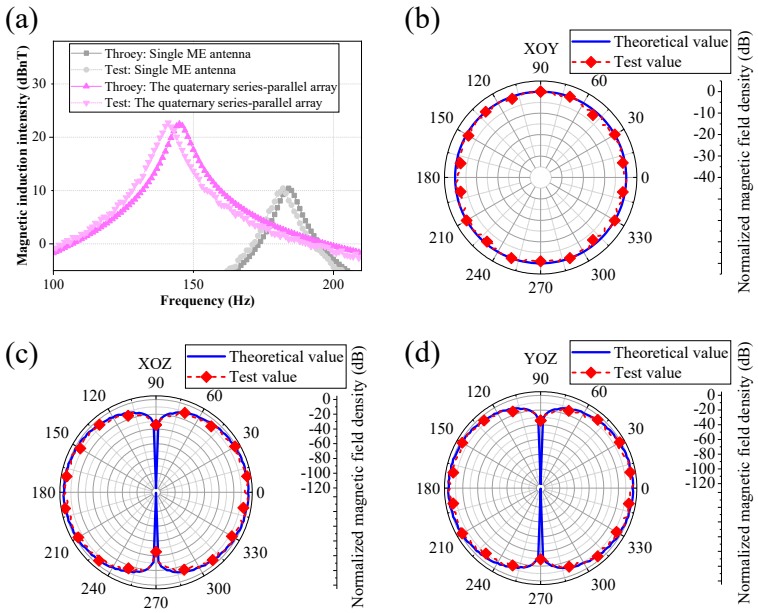

Figure 13. Test results of quaternary series–parallel stack array of ME antenna: (**a**) The frequency response of the quaternary series–parallel stack array of ME antenna. (**b**) The radiation pattern of the XOY plane. (**c**) The radiation pattern of the XOZ plane. (**d**) The radiation pattern of the YOZ plane.

5. Conclusions

The three experimental results were verified according to the theoretical results, which fully proved that the ME antenna arrays are effective and reliable for the adjustment of frequency response and the improvement of radiation intensity. The proposed equivalent circuit can accurately calculate the frequency response and EMV of the ME antenna array.

This work is aimed at further investigating and optimizing the ME antenna array methodology. We report the characterization and accurate circuit modeling of three small ME antenna arrays. The mechanical parameters allow accurate calculation of the frequency response and EMV of the ME antenna and its arrays.

In practical applications, these small arrays can replace a single ME antenna and become the element of a large array. Without affecting the overall size of the large array, the frequency response of the large array can be adjusted, and the radiation intensity of the large array can have multiple improvements. Among them, the fractional bandwidth of BSMEA can be extended to 8.3%. How to form the miniature magnetoelectric arrays described in this paper into large arrays and thus enhance the radiation distance will be the focus of future work. Taking advantage of the larger fractional bandwidth provided by micro arrays to achieve higher information transfer rates is also one of the research hotspots. Higher fractional bandwidth provides the hardware basis for subsequent efficient information loading.

These ME antenna arrays have positive implications for SLF magnetic induction communication systems.

Author Contributions: Conceptualization, S.W. and G.D.; methodology, S.W. and G.D.; software, S.W. and G.D.; validation, S.W. and G.S.; formal analysis, G.S.; investigation, G.S.; resources, S.W.; writing— original draft preparation, S.W.; writing—review and editing, S.W. and G.D.; visualization, S.W. and G.S.; supervision, S.W. and G.D. All authors have read and agreed to the published version of the manuscript.

Funding: This research was funded by the National Natural Science Foundation of China, grant number 61871473.

Data Availability Statement: Datasets available upon request from the authors.

Acknowledgments: The authors sincerely thank the editors and reviewers for their kind attention and valuable comments dedicated to this paper.

Conflicts of Interest: The authors declare no conflicts of interest.

References

1. Ahmed, I.; Andrew, S.; Saher, S. Propagation of Electromagnetic Waves at MHz Frequencies Through Seawater. *IEEE Trans. Antennas Propag.* **2004**, *52*, 2843–2849.
2. Muhammad, T.; Piao, Y.; Liu, S. Channel characterization of EM waves propagation at MHz frequency through seawater. *Int. J. Commun. Syst.* **2017**, *31*, 1–15.
3. Wang, H.; Zhang, K.; Yang, K.; Ma, Y. Electromagnetic field in air produced by a horizontal magnetic dipole immersed in sea: Theoretical analysis and experimental results. *IEEE Trans. Antennas Propag.* **2014**, *62*, 4647–4655. [CrossRef]
4. John, P.; Yahya, R. Fractal antennas: A novel antenna miniaturization technique, and applications. *IEEE Antennas Propag. Magn.* **2002**, *44*, 20–36.
5. Liang, Y.; Zheng, X. Experimental researches on magneto-thermo-mechanical characterization of terfenol-D. *Acta Mech. Solida Sin.* **2007**, *20*, 283–288. [CrossRef]
6. Nan, C.; Bichurin, M.; Dong, S.; Viehland, D.; Srinivasan, G. Multiferroic magnetoelectric composites: Historical perspective, status, and future directions. *J. Appl. Phys.* **2008**, *3*, 031101. [CrossRef]
7. Gillette, S.; Geiler, A.; Gray, D.; Viehland, D.; Vittoria, C.; Harris, V. Improved sensitivity and noise in magnetoelectric magnetic field sensors by use of modulated AC magnetostriction. *IEEE Magn. Lett.* **2011**, *2*, 2500104. [CrossRef]
8. Jahns, R.; Greve, H.; Woltermann, E.; Quandt, E.; Kncöhel, R. Sensitivity enhancement of magnetoelectric sensors through frequency-conversion. *Sens. Actuators A Phys.* **2012**, *183*, 16–21. [CrossRef]
9. Suzuki, M.; Wada, T.; Takahashi, T.; Nishida, T.; Aoyagi, S. Nano-porous SiO_2 electret with high surface potential and high thermal resistance. In Proceedings of the 2014 IEEE 27th International Conference on Micro Electro Mechanical Systems (MEMS), San Francisco, CA, USA, 26–30 January 2014; pp. 417–420.
10. Nan, T.; Lin, H.; Gao, Y.; Matyushov, A. Acoustically actuated ultra-compact NEMS magnetoelectric antennas. *Nat. Commun.* **2017**, *8*, 296. [CrossRef]
11. Bickford, J.; Duwel, A.; Weinberg, M.; McNabb, R. Performance of electrically small conventional and mechanical antennas. *IEEE Trans. Antennas Propag.* **2019**, *67*, 2209–2223. [CrossRef]
12. Cui, Y.; Wang, C.; Song, X.; Wu, M.; Zhang, Q.; Yuan, H.; Yuan, Z. A survey of mechanical antennas applied for low-frequency transmitting. *Iscience* **2022**, *26*, 1. [CrossRef]
13. Xu, R.; Tiwari, S.; Candler, R.; Chen, S. Polarization control of bulk acoustic wave-mediated multiferroic antennas based on thickness shear modes. In Proceedings of the 12th European Conference on Antennas and Propagation (EuCAP 2018), London, UK, 9–13 April 2018; pp. 1–5.
14. Xu, J.; Leung, C.; Zhuang, X.; Li, J.; Bhardwaj, S.; Volakis, J.; Viehland, D. A low frequency mechanical transmitter based on magnetoelectric heterostructures operated at their resonance frequency. *Sensors* **2019**, *19*, 853. [CrossRef]
15. Kemp, M.; Franzi, M.; Haase, A.; Jongewaard, E.; Whittaker, M.; Kirkpatrick, M.; Sparr, R. A high Q piezoelectric resonator as a portable VLF transmitter. *Nat. Commun.* **2019**, *10*, 1. [CrossRef]
16. Schneider, J.; Domann, J.; Panduranga, M.; Tiwari, S.; Carman, G. Experimental demonstration and operating principles of a multiferroic antenna. *J. Appl. Phys.* **2019**, *126*, 224104. [CrossRef]
17. Dong, C.; Wang, X.; Lin, H.; Gao, Y.; Zaeimbashi, M. A portable very low frequency (VLF) communication system based on acoustically actuated magnetoelectric antennas. *IEEE Antennas Wirel. Propag. Lett.* **2020**, *19*, 398–402. [CrossRef]
18. Drobitch, J.; De, A.; Dutta, K.; Pal, K.; Adhikari, A.; Barman, A. Extreme subwavelength magnetoelastic electromagnetic antenna implemented with multiferroic nanomagnets. *Adv. Mater. Tech.* **2020**, *5*, 1–8.
19. Hassanien, A.; Breen, M.; Li, M.; Gong, S. Acoustically driven electromagnetic radiating elements. *Sci. Rep.* **2020**, *10*, 1–12.
20. Niu, Y.; Ren, H. Transceiving signals by mechanical resonance: A miniaturized standalone low frequency (LF) magnetoelectric mechanical antenna pair with integrated DC magnetic bias. *IEEE Sens. J.* **2022**, *22*, 14008–14017. [CrossRef]
21. Du, Y.; Xu, Y.; Wu, J.; Qiao, J.; Wang, Z.; Hu, Z.; Jiang, Z.; Liu, M. Very-Low-frequency magnetoelectric antennas for portable underwater communication: Theory and experiment. *IEEE Trans. Antennas Propag.* **2023**, *71*, 2167–2181. [CrossRef]
22. Yu, H.; Zeng, M.; Wang, Y.; Wan, J.; Liu, J. Magnetoelectric resonance-bandwidth broadening of Terfenol-D/epoxy-Pb(Zr, Ti)O_3 bilayers in parallel and series connections. *Appl. Phys. Lett.* **2005**, *86*, 1–4. [CrossRef]
23. Li, H.; Chen, S.; Zou, Z.; Yang, Y.; Zhu, B. Microbridge-structured magnetoelectric sensor array based on PZT/FeCoSiB thin films. *IEEE Trans. Magn.* **2020**, *56*, 4000504. [CrossRef]
24. Zhang, Y.; Jing, L.; Shi, P.; Hou, J.; Yang, X.; Peng, Y.; Chen, S. Research on a miniaturized VLF antenna array based on a magnetoelectric heterojunction. *J. Mater. Sci. Mater. Electron.* **2022**, *33*, 11–24. [CrossRef]

25. Prasad, M.; Tok, R.; Fereidoony, F.; Wang, Y.; Zhu, R.; Propst, A.; Bland, S. Magnetic pendulum arrays for efficient ULF transmission. *Sci. Rep.* **2019**, *9*, 1–13.
26. Fereidoony, F.; Prasad, M.; Santos, J.; Wang, Y. Efficient ULF transmission utilizing stacked magnetic pendulum array. *IEEE Trans. Antennas Propag.* **2022**, *70*, 585–597. [CrossRef]
27. Rocha, R.; ManoelTusset, J.; Souza, A. On a non-ideal magnetic levitation system: Nonlinear dynamical behavior and energy harvesting analyses. *Nonlinear Dyn.* **2019**, *95*, 3423–3438. [CrossRef]
28. Kecik, K.; Kowalczuk, M. Effect of nonlinear electromechanical coupling in magnetic levitation energy harvester. *Energies* **2021**, *14*, 2715. [CrossRef]
29. Rotanova, T.; Korobeynikov, S.; Larichkin, A. Hyperelasticity models extending Hooke's law from the region of small strains to moderate ones. In Proceedings of the International Conference Of Numerical Analysis And Applied Mathematics ICNAAM, Rhodes, Greece, 23–28 September 2020; pp. 1–5.
30. Piotr, K.; Jan, M. Two Masses in Relative Hooke's Potential and Elliptic Integrals. *J. Nonlinear Math. Phys.* **2022**, *29*, 504–522.
31. Mohamad, H.; Richard, W. Added mass and damping forces of a floating tidal turbine undergoing pendulum motion. *Ocean Eng.* **2023**, *283*, 1–9.
32. Li, X.; Zhang, R.; Wan, C.; Xue, S.; Xie, L.; Tong, Y. Additional damping force identification of passively controlled structures based on a Gillijn De Moor filter. *Measurement* **2023**, *224*, 1–9. [CrossRef]
33. Yang, W.; Zhang, H.; Chen, Z.; Hua, X.; Niu, H. Study on enhanced performance of CuFe alloy's eddy current damping and its advantages in multi-mode vibration control of stay-cable. *Eng. Struct.* **2023**, *299*, 1–17. [CrossRef]

Disclaimer/Publisher's Note: The statements, opinions and data contained in all publications are solely those of the individual author(s) and contributor(s) and not of MDPI and/or the editor(s). MDPI and/or the editor(s) disclaim responsibility for any injury to people or property resulting from any ideas, methods, instructions or products referred to in the content.